Scientific Research Publishing

Crystal Structure Theory and Applications, 2020, 9, 1-11
https://www.scirp.org/journal/csta
ISSN Online: 2169-2505
ISSN Print: 2169-2491

Investigation of Inhomogeneity in Single Crystal SiC Wafers Using C-Scan Acoustic Scanning Microscopy

Ibrahim M. Abdel-Motaleb

Department of Electrical Engineering, Northern Illinois University, DeKalb, IL, USA
Email: ibrahim@niu.edu

How to cite this paper: Abdel-Motaleb, I.M. (2020) Investigation of Inhomogeneity in Single Crystal SiC Wafers Using C-Scan Acoustic Scanning Microscopy. *Crystal Structure Theory and Applications*, **9**, 1-11.
https://doi.org/10.4236/csta.2020.91001

Received: November 27, 2019
Accepted: February 24, 2020
Published: February 27, 2020

Abstract

In this work, C-Scan Acoustic Scanning Microscopy (ASM) is used to map the defects of three SiC samples. The acoustic images indicate that numerous defects with different shapes and area sexist in the wafers. Some of the defects have areas of more than 100,000 μm^2. The number of defects ranges from 1 to 50 defects/wafer. Defect mapping is essential for defect repairing or avoidance. This work shows that ASM can locate the precise positions of the crystallographic defects, which enables defects repair and yield enhancement.

Keywords

SiC, Lattice Defects, Acoustic Scanning Microscopy, ASM, Wafers

1. Introduction

Silicon Carbide material has become one of the critical materials in the microelectronics industry. SiC has many properties that are hard to find in a single semiconducting material. It is a wide band gap material that can be used to build blue, green, or white optoelectronic devices [1] [2] [3]. Additionally, SiC is widely used to build power electronic devices, such as Bipolar Junction Transistors (BJT) and Field Effect Transistors (FETs) for high voltage applications [4] [5] [6] [7] [8]. It is also used to build FETs for digital, analog, and microwave applications [9] [10] [11].

SiC crystals are grown at temperatures up to more than 1600˚C [12]. Crystal growth at these high temperatures can cause many intrinsic defects including missing atoms, displaced atoms, missing stacks of atoms, micro-pipes, screw dislocations, line defects, and point defects [13] [14]. These defects can result in device failure, performance degradation [15], low reliability and sensitivity to

self-heating [10].

Several techniques have been used to study defects in semiconductor substrates, including SiC wafers. Among these are photomicrography and scanning electron microscopy (SEM). These techniques are effective in identify surface defects. Bulk defects can be identified using techniques such as Optical Coherence Tomography (OCT) that can detect defects on the surface and in the bulk [16]. However, OTC requires the transmission of the light into the material, which may not be possible for less transparent materials. Raman spectroscopy is another technique that can provide information about the lattice structural and electrical properties of the material [17]. But, its mapping capability remains a problem. Selective etching is used to reveal the exact location of the defects [18]. However, this technique is destructive. White-beam synchrotron topography has been also used to study defects in SiC [19] [20]. This technique is costly with safety concerns. Deep Level Transient Spectroscopy (DLTS) is another technique to be used to study defects in SiC, as it was used in GaAs and other semiconductor materials [21] [22]. This technique is less costly, but it provides information about the energy level of the defects not their locations. As can be seen from above, the main problem of these techniques is that they suffer from one or more shortcomings. They may be expensive, destructive, unable to map defects, or cannot locate defects residing inside the material.

Acoustic Scanning Microscopy (ASM) is a viable alternative to the above techniques. It is a very cost-effective technique that can provide scanning for the crystal defects to determine their exact locations, shapes, and areas. Knowing the X-Y location allows for a targeted repair or avoidance of defects. Knowing the Z-location can help in determining the type and value of energy required for the repair. ASM is also used in imaging the samples to determine voids, cracks, and inhomogeneity inside the materials. One of the advantages of ASM is that it can be used for all types of materials such as, semiconductor, crystalline, amorphous, polycrystalline, metallic, insulator, nonmetallic, biological, or organic material.

In 1959, Dunn and Fry demonstrated the first experiment of acoustic microscopy [23]. Acoustic microscopy has been proposed for tissue characterization by Kessler and Yuhas [24]. The C-Scam ASM was developed by Kessler and others in the 1980's [25]. ASM can be performed using reflected or transmitted signals. In this study, the reflected echo microscopy is used. A detailed information about acoustic microscopy can be found in the book authored by Briggs and Kolosove [26].

Acoustic scanning microscopes use acoustic frequencies ranging from 5 - 500 MHz. The frequency of high speed microscopecan reach up to 2 GHz. Low frequency waves can penetrate deeper in the sample, but has lower imaging resolution. On the other hand, high frequency waves penetration is shallower, but their resolution is higher, reaching the micron level. One of the advantages of ASM is that the samples do not need special preparation for scanning, as long as it can withstand water or other acoustically conductive liquid. Acoustic conductive medium is needed for interfacing the sample with the signal. Air is a poor conduc-

tor, and is not an effective interfacing medium.

At any interface, the reflected portion of the signal depends on the acoustic impedance of the material at the two sides of the interface. If Z_1 and Z_2 are the impedance of material 1 and material 2 of the interface, then the reflection R can be obtained from the equation:

$$R = \frac{Z_2 - Z_1}{Z_2 + Z_1}$$

By detecting the intensity of the reflected acoustic signal, an image of the scanned material can be obtained. If the surface of the sample is smooth, then the intensity of the reflected signal will be uniform, and the image will show no irregularity. However, if the signal meets an interface with different materials, part of the signal will be reflected. Using the reflected signal, an image of the irregularities is created. Similarly, an image is created, if there is a defect or a crack inside the material. In this case, a large portion of the signal (close to 100%) will be reflected since the defect or the crack is filled either with air or is a void of any substance. The position of the beam determines the X-Y coordinates of the defect. The time that the reflected beam takes to reach the sensor determines the depth at which the defect resides. Therefore, the system can determine the X, Y, Z coordinates of the defects.

In this study, C-scan ASM is used to identify the X-Y coordinates of surface and bulk defects. This identification is critical, since it provides an accurate information about the locations and the shapes of the defects, irregularities, or discontinuities. In this study, three SiC wafers are scanned and imaged. The defects are mapped for each sample. The samples used are a) Semi-insulating 6H-SiC, b) N-doped 6H-SiC, and c) N-doped 4H-SiC.

2. Experimental Results and Analysis

In this study, KSI-V8 [27], high-speed scanning acoustic microscope, is used to image and map the defects of three SiC wafers. The wafers are purchased from Cree Inc. This acoustic microscope can perform a nondestructive testing, imaging, and characterization at frequencies up to 500 MHz. Therefore, this microscope is capable of a resolution in the micrometer range. The maximum scan field is 400 × 400 mm^2 and the maximum magnification is 625x.

The test was performed on three 3-inch samples. These samples are shown in **Figure 1**. Sample-1 is a semi-insulating 6H SiC wafer with a clear color. Sample-2 is a N-doped 6H SiC wafer with a green/blue color. Sample-3 is a N-doped 4H SiC wafer with a gray color. The objective of the study is to detect, map, and visualize defects in the "Pulse Echo Mode".

Figure 2(a) shows a C-scan of Sample-1, where the location and the shape of three defects are shown. **Figure 2(b)** shows the details of one defect that has a radius of 214 μm. **Figure 2(c)** shows a B-scan magnifying the X-Z axes image, with the Time of Flight (TF) indicated on the image as 63 ns. Since the objective of this study is to map the defects, C-scan will be used subsequently.

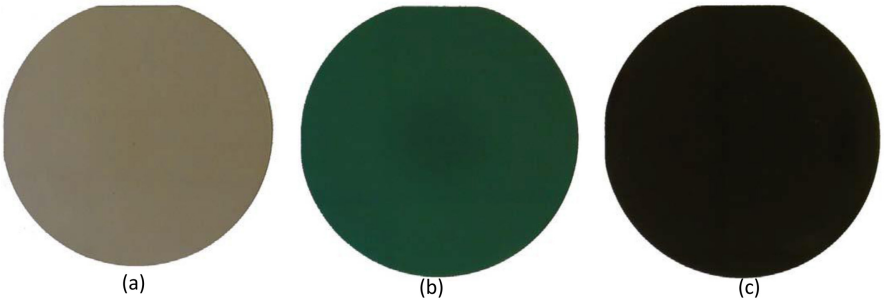

Figure 1. (a) Sample-1: X-70114230; clear, 6H SiC-Semi-insulating. (b) Sample 2: X-70114231, blue/green, N-doped 6H SiC. (c) Sample 3: X-70114232, gray, N-doped 4H SiC-N.

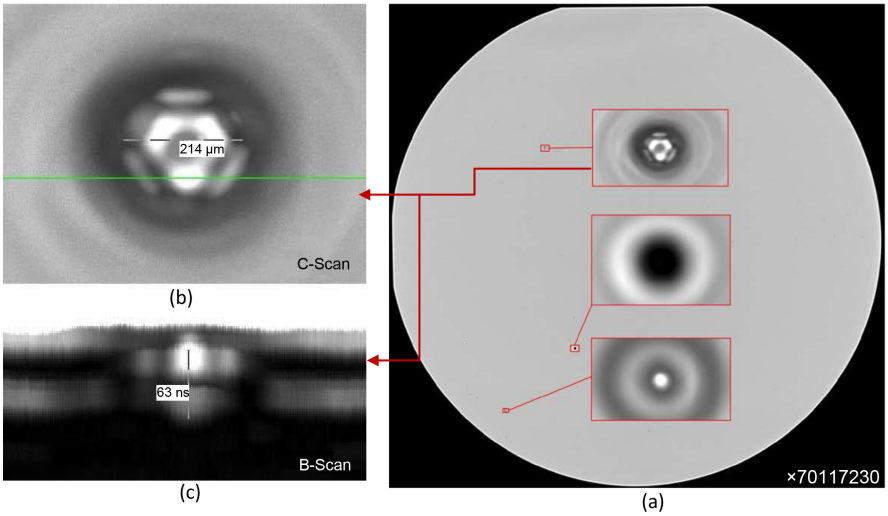

Figure 2. (a) C-scan of Sample 1 showing 3 defects with zoomed images. (b) Magnified C-scan showing a defect with a diameter size of 214 µm. (c) B-scan showing a time of flight of 63 ns that determinesthe X-Z axes image.

The defects of Sample-1 are mapped, as shown in **Figure 3**. This sample is a semi-insulating crystal. The mapping shows that there are 37 defects in the 3-inch area. These defects are assumed to be intrinsic vacancies, deviancies, and other defects created during the material growth. **Figure 4** shows the shape of the defects of Sample-1. **Table 1** shows the area and the X-Y position of each defect. In all mapping, upper left corner of the graph is considered the origin of the X-Y axes. The defects are named as P1R1 to P1R37. The shapes and areas of the defects vary. The defects take different shapes, as shown in **Figure 4**. The size of the areas ranges from 0.0007 to 0.1238 mm^2 for defect P1R3 and P1R31. **Figure 5** shows the defect mapping of Sample-2 and **Figure 6** shows the shapes of the defects. **Table 2** shows the area and the X-Ycoordinates for each defect. The wafer has 50 defects with defect areas ranging from 0.0007 to 0.1017 mm^2. This sample is 6H, N-type SiC. The larger number of defects could be intrinsic defects, similar to Sample-1, with other defects due to doping. The density of defects for Samples-1 & 2 are high that renders the wafers unsuitable for electronic fabrication. For these wafers to be used, recrystallization to remove the defects needs to be performed.

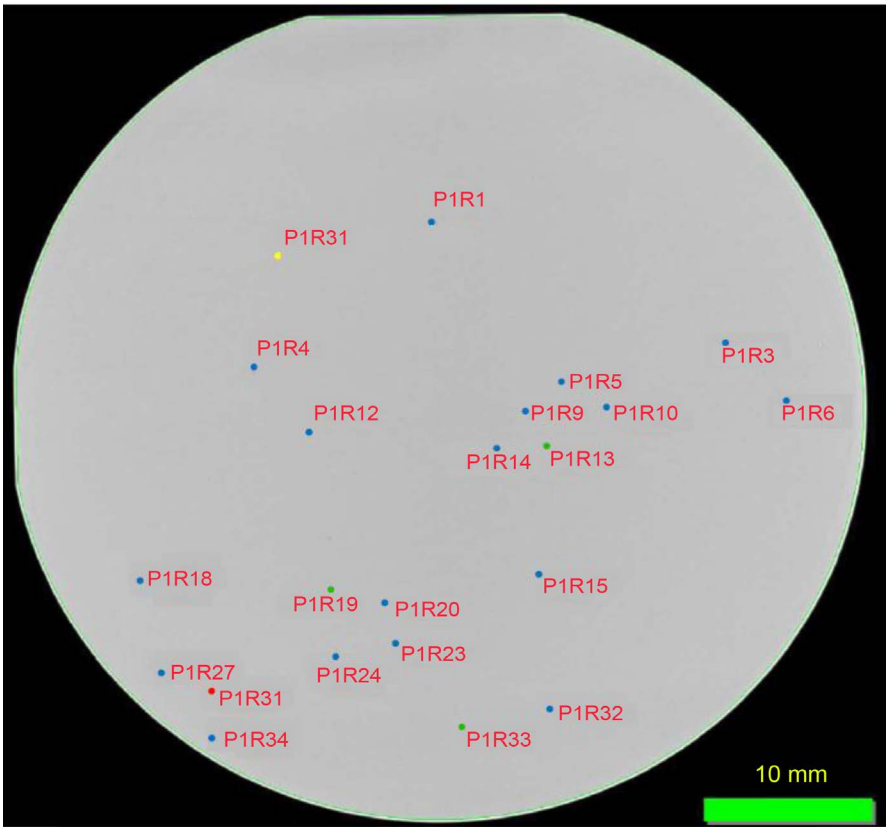

Figure 3. Mapping of defects of Sampe-1. Semi-insulating undoped 6H SiC.

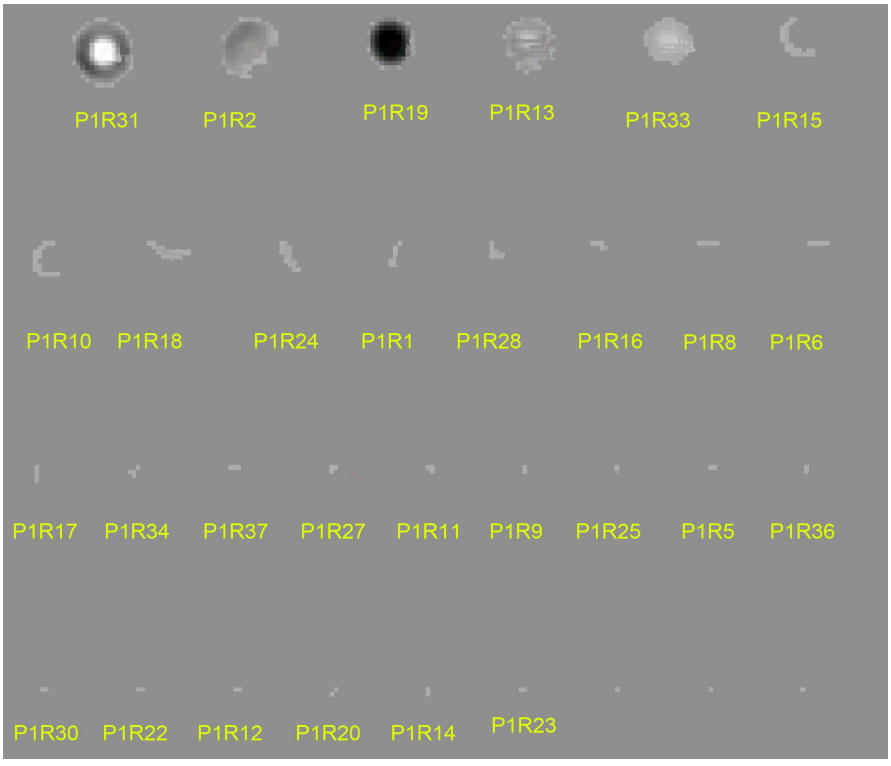

Figure 4. Magnified images of the defects in Samp1e-1. Images are arranged according to their area.

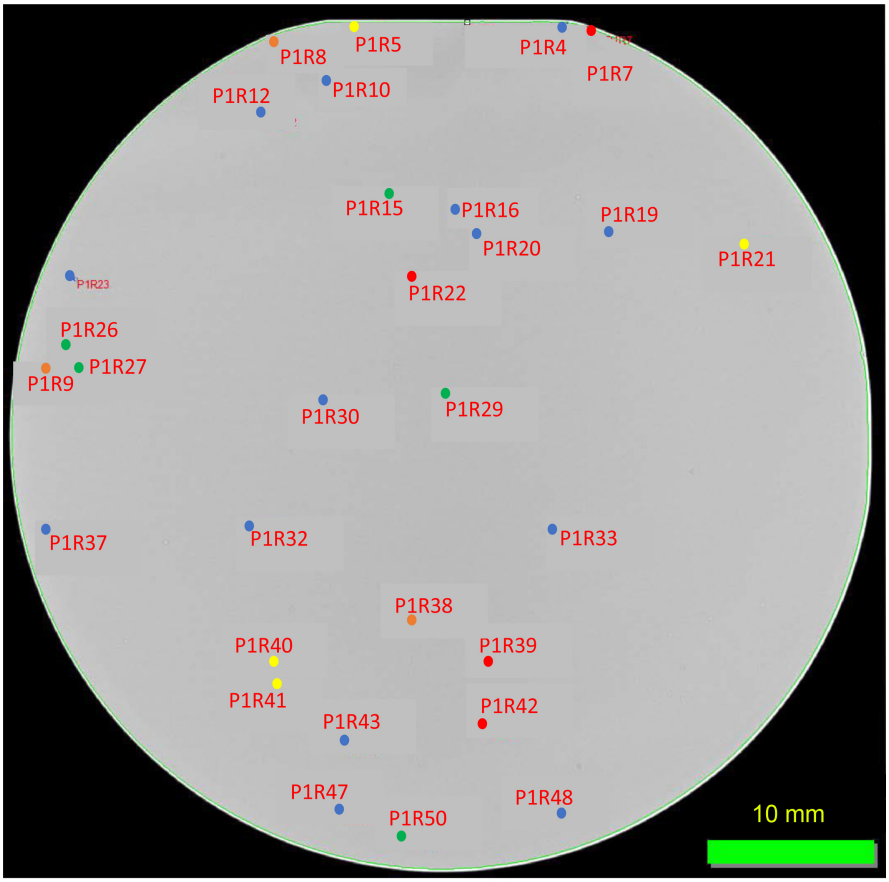

Figure 5. Mapping of defects of Sampe-2, N-doped 6H SiC.

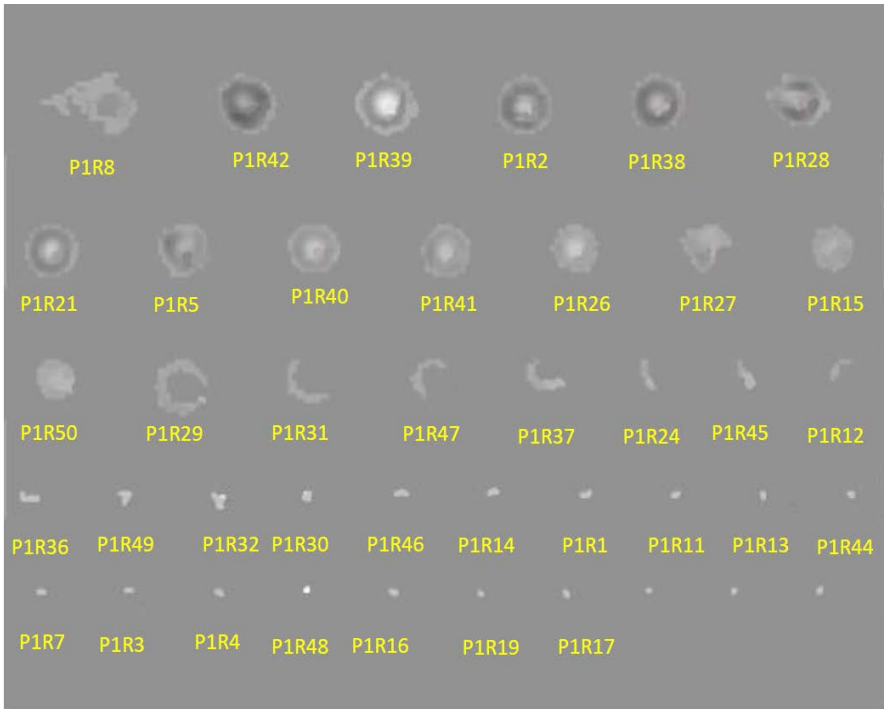

Figure 6. Magnified images of the defects in Samp1e-2. Images are arranged according to the defect area.

Table 1. Coordinates and areas of defects in Sample-1, 6H Semi-insulation SiC.

Feature Name	Area (mm^2)	Centroid Pixel X (mm)	Centroid Pixel Y (mm)	Feature Name	Area (mm^2)	Centroid Pixel X (mm)	Centroid Pixel Y (mm)
P1R1	0.0056	25.9643	13.4598	P1R20	0.0014	23.1778	36.7434
P1R2	0.0916	16.9371	15.2055	P1R21	0.0007	23.1382	36.8361
P1R3	0.0007	43.3411	20.9169	P1R22	0.0014	23.2307	36.8889
P1R4	0.0007	15.4431	22.4242	P1R23	0.0014	23.8654	39.2688
P1R5	0.0014	33.6495	23.2968	P1R24	0.0119	20.1936	39.9796
P1R6	0.0035	46.9374	24.3017	P1R25	0.0014	20.4145	39.9166
P1R7	0.0007	46.8317	24.3811	P1R26	0.0007	20.4145	39.9828
P1R8	0.0035	46.9111	24.4604	P1R27	0.0021	9.8194	40.9435
P1R9	0.0014	31.4415	24.8438	P1R28	0.0049	9.7993	41.0934
P1R10	0.0133	36.2974	24.9322	P1R29	0.0007	9.9957	41.0405
P1R11	0.0021	36.4305	24.8658	P1R30	0.0014	9.9031	41.1463
P1R12	0.0014	18.7089	26.2851	P1R31	0.1238	12.8922	42.3511
P1R13	0.0755	32.6748	27.1434	P1R32	0.0007	32.9752	43.2882
P1R14	0.0014	29.8284	27.2502	P1R33	0.0629	27.6874	44.4767
P1R15	0.0182	32.1687	34.9605	P1R34	0.0028	12.8516	45.0599
P1R16	0.0035	32.3035	34.8368	P1R35	0.0007	13.0103	45.0599
P1R17	0.0028	32.3405	34.9452	P1R36	0.0014	12.8516	45.1789
P1R18	0.0126	8.6265	35.4581	P1R37	0.0021	12.9309	45.2451
P1R19	0.0762	20.0455	35.9209				

Figure 7 shows the mapping of the defects for Sample-3, N-doped 4H SiC. For this sample there is only one defect. This shows that this sample has little intrinsic or doping defects. Figure 8, shows the shape of the defect. As indicated in Table 3, the area of the defect is 0.1045 mm^2. The difference between the samples is, more likely a result of the place of the sample in the ingot, although the type of the crystal, 6H vs. 4H, could be also a factor.

3. Conclusions

To the best of my knowledge, this is one of the few studies of defects in SiC substrates using ASM, if not the only one. The study suggests that defects can take any shape and cover an area greater that 0.1 mm^2 or a circular area of more than 300 μm diameter. Such defects render the wafer unusable for device or integrated circuit manufacturing, without some sort of repair.

This study can open the door for developing new processes and instruments. First, the study shows that ASM technique is a cost effective technique to evaluate

Table 2. Coordinates and areas of defects in Sample-2, N-doped 6H SiC.

Feature Name	Area (mm^2)	Centroid Pixel X (mm)	Centroid Pixel Y (mm)	Name	Area (mm^2)	Centroid Pixel X (mm)	Centroid Pixel Y (mm)
P1R1	0.0021	26.8698	1.0758	P1R26	0.0631	3.7072	19.5456
P1R2	0.0007	26.9978	1.0758	P1R27	0.0545	4.6347	20.7806
P1R3	0.0013	27.7022	1.0758	P1R28	0.0861	2.6025	20.8651
P1R4	0.0013	32.7996	1.1014	P1R29	0.0413	25.7208	22.3303
P1R5	0.0761	20.5087	1.2854	P1R30	0.0021	18.4511	22.6775
P1R6	0.0007	34.6311	1.6137	P1R31	0.0184	18.4124	22.8693
P1R7	0.0013	34.9001	1.7162	P1R32	0.0033	14.5031	29.8206
P1R8	0.1017	15.7376	1.9783	P1R33	0.0007	31.8391	29.8667
P1R9	0.0007	11.6547	4.0215	P1R34	0.0007	31.9671	29.8923
P1R10	0.0007	19.4415	4.1496	P1R35	0.0007	31.7622	29.9947
P1R11	0.0007	19.0957	4.7131	P1R36	0.0033	31.8441	30.0665
P1R12	0.0059	15.0956	6.3695	P1R37	0.0144	2.6779	30.2008
P1R13	0.0013	15.2919	6.4677	P1R38	0.0886	23.8431	35.4055
P1R14	0.0021	15.1895	6.5317	P1R39	0.0971	28.4035	37.5663
P1R15	0.0518	22.5017	11.0117	P1R40	0.0755	15.9323	37.6272
P1R16	0.0013	26.2422	11.8596	P1R41	0.0748	16.1312	38.7997
P1R17	0.0013	26.2294	11.9236	P1R42	0.0984	27.8038	41.2025
P1R18	0.0007	26.4087	12.0133	P1R43	0.0007	20.0563	42.1873
P1R19	0.0013	35.2201	13.1531	P1R44	0.0013	20.1971	42.2129
P1R20	0.0007	27.6638	13.3708	P1R45	0.0059	20.0278	42.3296
P1R21	0.0821	43.1088	13.6922	P1R46	0.0021	20.1331	42.3922
P1R22	0.0925	24.0271	15.6237	P1R47	0.0151	19.6487	46.2667
P1R23	0.0007	4.2264	15.6505	P1R48	0.0013	32.6331	46.3241
P1R24	0.0085	4.1752	15.7767	P1R49	0.0033	19.7284	46.3984
P1R25	0.0007	4.3801	15.7531	P1R50	0.0446	23.3372	47.5939

Table 3. Coordinates and areas of defects in Sample-3, N-doped 4H SiC.

Feature Name	Area (mm^2)	Centroid Pixel X (mm)	Centroid Pixel Y (mm)
P1R1	0.1045	6.7782	38.2852

the quality of the growth process by characterizing the defect density along the ingot. The study highlights the need for new ASM microscopes, with laser repairing capability. The new instruments would be able to perform investigation of defect repairing process and thermal stress impact on the repaired substrates.

Using both B and C scan microscopy, laser energy and wavelength, that ensure the best recrystallization results, can be determined. C scan determines the

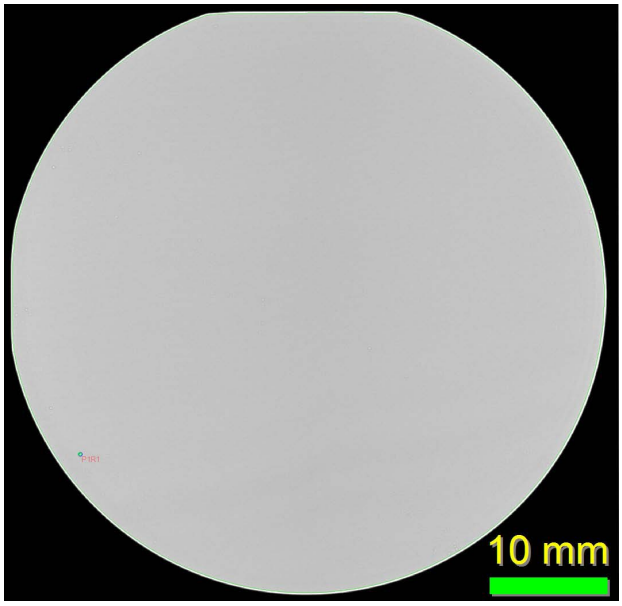

Figure 7. Mapping of defects of Sampe-3, N-doped 4H SiC.

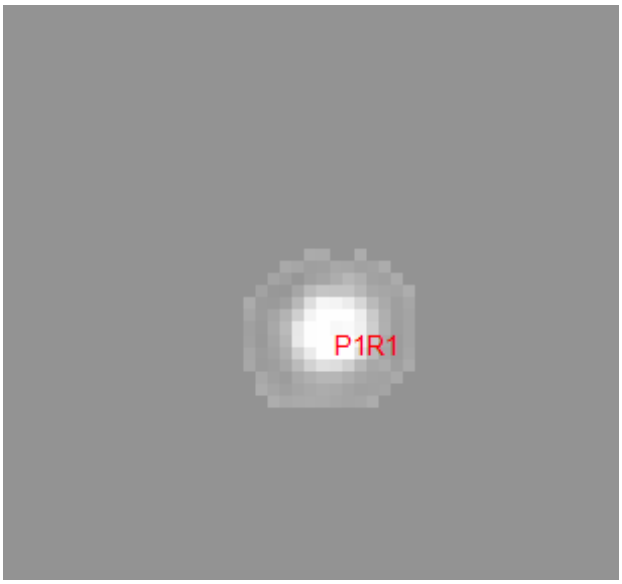

Figure 8. Magnified images of the defects in Samp1e-3. Images are arranged according to the defect area.

location and the area, and B scan determines the defects Z-locations and thicknesses. With this information, the wave length capable of penetration the material to that depth can be determined, and the energy needed to repair the specific defect size can be estimated. In fact, these proposed methods and instruments can be adopted for other substrates and materials.

Conflicts of Interest

The author declares no conflicts of interest regarding the publication of this paper.

References

[1] Niina, T., Ohta, K., Nakata, T., Matsushita, Y., Uetani, T. and Fujikawa, Y. (1993) Light Emitting Diode Device and Method for Producing Same. US Patent No. 5187547.

[2] Edmond, J.A. and Suvorov, A.V. (1997) Method of Forming Green Light Emitting Diode in Silicon Carbide. US Patent No. 5604135.

[3] Chiu, C.-C., Chen, C.-L. and Shih, K.-K. (2003) High Efficiency White Light Emitting Diode. US Patent No. 6614172B2.

[4] Zhang, Q., Callanan, R., Das, M.K., Ryu, S.-H., Agarwal, A.K. and Palmour, J.W. (2010) SiC Power Devices for Microgrids. *IEEE Transaction on Power Electronics*, **25**, 2829-2896. https://doi.org/10.1109/TPEL.2010.2079956

[5] Östling, M., Ghandi, R. and Zetterling, C.-M. (2011) SiC Power Devices-Present Status, Applications and Future Perspective. *Proceedings IEEE 23rd International Symposium on Power Semiconductor Devices and ICs*, San Diego, CA, 23-26 May 2011. https://doi.org/10.1109/ISPSD.2011.5890778

[6] Thakkallapally, R., Veesam, V., Abdel-Motaleb, I. and Shen, Z. (2014) One-Directional 3D-SiC MESFET for High Power Applications. *Proceedings of the IEEE National Aerospace and Electronic Conference*, Dayton, OH, 24-27 June 2014. https://doi.org/10.1109/NAECON.2014.7045766

[7] Veesam, V., Thakkallapally, R., Abdel-Motaleb, I. and Shen, Z. (2015) Evaluation of Electric Field and Temperature of 3D SiC/Si Normally-off MOSFET for High Power High Speed Applications. *Proceedings of the IEEE Electro-Information Technology IEEE-EIT*, Naperville, IL, 21-23 May 2015. https://doi.org/10.1109/NAECON.2014.7045767

[8] Thakkallapally, R., Veesam, V., Abdel-Motaleb, I. and Shen, Z. (2015) Electrical and Thermal Analysis of Vertical Unidirectional 3C-SiC MESFETs on Silicon Substrate. *Proceedings of the IEEE Electro-Information Technology IEEE-EIT*, Naperville, IL, 21-23 May 2015. https://doi.org/10.1109/EIT.2015.7293416

[9] Henry, H.G., Augustine, G., DeSalvo, G.C., Brooks, R.C., Barron, R.R., Oliver, J.D., Morse, A.W., Veasel, B. W., Esker, P.M. and Clarke, R.C. (2004) S-Band Operation of SiC Power MESFET with 20 W (4.4 W/mm) Output Power and 60% PAE. *IEEE Transaction on Electron Devices*, **51**, 839-845. https://doi.org/10.1109/TED.2004.828279

[10] Asmi, S. and Abdel-Motaleb, I.M. (2006) Effect of Traps and Self Heating on the Microwave Performance of SiC MESFETs. *The 8th International Conference on Solid State and Integrated Circuit Technology*, Shanghai, China, 23-26 October 2006. https://doi.org/10.1109/ICSICT.2006.306553

[11] Ouaida, R., Berthou, M., León, J., Perpiñà, X., Oge, S., Brosselard, P. and Joubert, C. (2014) Gate Oxide Degradation of SiC MOSFET in Switching Conditions. *IEEE Electron Devices Letters*, **35**, 1284-1286. https://doi.org/10.1109/LED.2014.2361674

[12] Leone, S., Beyer, F.C., Pedersen, H., Andersson, S., Kordina, O., Henry, A. and Janzén, E. (2011) Chlorinated Precursor Study in Low Temperature Chemical Vapor Deposition of 4H-SiC. *Thin Solid Film*, **519**, 3074-3080. https://doi.org/10.1016/j.tsf.2010.12.119

[13] Chien, F.R., Ning, X.J., Stemmer, S. and Pirouz, P. (1996) Growth Defects in GaN Films on 6H-SiC Substrates. *Applied Physics Letters*, **68**, 2678. https://doi.org/10.1063/1.116279

[14] Kong, H.S., Glass, J.T. and Davis, R.F. (1989) Growth Rate, Surface Morphology,

and Defect Microstructures of β-SiC Films Chemically Vapor Deposited on 6H-SiC Substrates. *Journal of Material Research*, **4**, 204-214. https://doi.org/10.1557/JMR.1989.0204

[15] Kimoto, T., Miyamoto, N. and Matsunami, H. (1999) Performance Limiting Surface Defectsin SiC Epitaxial p-n Junction Diodes. *IEEE Transactions on Electron Devices*, **46**, 871-477. https://doi.org/10.1109/16.748864

[16] Duncan, M.D. and Bashkansky, M. (1998) Subsurface Defect Detection in Materials Using Optical Coherence Tomography. *Optical Express*, **2**, 540-545. https://doi.org/10.1364/OE.2.000540

[17] Nakashima, S. and Harima, H. (2004) Characterization of Defects in SiC Crystals by Raman Scattering. In: Choyke W.J., Matsunami, H. and Pensl, G., Eds., *Silicon Carbide. Advanced Texts in Physics*, Springer, Berlin, Heidelberg. https://doi.org/10.1007/978-3-642-18870-1_24

[18] Weyher, J.L. (2006) Characterization of Wide-Band-Gap Semiconductors (GaN, SiC) by Defect-Selective Etching and Complementary Methods. *Superlattices and Microstructures*, **40**, 279-288. https://doi.org/10.1016/j.spmi.2006.06.011

[19] Dudley, M., Wang, S.P., Huang, W., Carter Jr., C.H., Tsvetkov, V.F. and Fazi, C. (1995) White-Beam Synchrotron Topographic Studies of Defects in 6H-SiC Single Crystals. *Journal of Physics D: Applied Physics*, **28**, A63-A67. https://doi.org/10.1088/0022-3727/28/4A/012

[20] Dudley, M., Huang, X. and Vetter, W.M. (2004) Synchrotron White Beam X-Ray Topography and High Resolution X-Ray Diffraction Studies of Defects in SiC Substrates, Epilayers and Device Structures. In: Choyke, W.J., Matsunami, H. and Pensl, G., Eds., *Silicon Carbide. Advanced Texts in Physics*, Springer, Berlin, Heidelberg. https://doi.org/10.1007/978-3-642-18870-1_26

[21] Dendo, S., Abdel-Motaleb, I., Lowe, K. and Young, L. (1985) Deep Levels in Semi-Insulating LEC GaAs before and after Silicon Implantation. *Journal of the Electrochemical Society*, **132**, 2673. https://doi.org/10.1149/1.2113646

[22] Hemmingsson, C., Son, N.T., Kordina, O., Bergman, J.P. and Janzén, E. (1997) Deep Level Defects in Electron-Irradiated 4H SiC Epitaxial Layers. *Journal of Applied Physics*, **81**, 6155. https://doi.org/10.1063/1.364397

[23] Dunn, F. (1959) Ultrasonic Absorption Microscope. *The Journal of the Acoustical Society of America*, **31**, 632. https://doi.org/10.1121/1.1907767

[24] Kessler, L.W. and Yuhas, D.E. (1979) Acoustic Microscopy. *Proceedings of the IEEE*, **67**, 526-536. https://doi.org/10.1109/PROC.1979.11281

[25] Semmens, J.E. and Kessler, L.W. (1989) Nondestructive Evaluation of TAB Bonding by Means of Acoustic Microscopy: Overview of Progress Using C-Mode Scanning Acoustic Microscopy. 9*th IEEE/CHMT*, *International Conference on Manufacturing Technology*, 12-17 February 1989.

[26] Briggs, G. and Kolosove, O. (2010) Acoustic Microscopy. 2nd Edition, Oxford University Press, Oxford.

[27] https://www.ksisam.com/acousticmicroscopy-en/home-acoustic-microscopy.php